Towards the 3D printing of innovative hydrogel scaffolds through vat polymerization techniques using methacrylated carboxymethylcellulose aqueous formulations

Lénaïc Soullard, Angélique Schlepp, Raphaël Buret, Christine Lancelon-Pin, Guillaume Nonglaton, Isabelle Texier, Bruno Jean, Sébastien Rolere

Towards the 3D printing of innovative hydrogel scaffolds through vat polymerization techniques using methacrylated carboxymethylcellulose aqueous formulations

Lénaïc Soullard[a,b,c], Angélique Schlepp[d], Raphaël Buret[a], Christine Lancelon-Pin[c], Guillaume Nonglaton[b], Isabelle Texier[b], Bruno Jean[c] and Sébastien Rolere*[a]

[a] *Univ. Grenoble Alpes, CEA, LITEN, DTNM, 17 avenue des Martyrs, 38000 Grenoble, France*
[b] *Univ. Grenoble Alpes, CEA, LETI, DTIS, 17 avenue des Martyrs, 38000 Grenoble, France*
[c] *Univ. Grenoble Alpes, CNRS, CERMAV, 601 Rue de la Chimie, 38400 Gières, France*
[d] *Microlight 3D, 5 Av. du Grand Sablon, 38700 La Tronche, France*

**Corresponding author: sebastien.rolere@cea.fr*

Abstract

Two vat polymerization techniques were evaluated to print innovative hydrogel scaffolds for tissue engineering, from aqueous photo-crosslinkable formulations based on methacrylated carboxymethylcellulose (mCMC). A first formulation containing 2 wt% mCMC with a methacrylation degree (DM) of 34 % and lithium phenyl-2,4,6-trimethylbenzoylphosphinate (LAP) as photoinitiator was specifically developed for Digital Light Processing (DLP). Considering their viscoelastic properties measured by shear rheology, the DLP-printed hydrogels were proposed for soft tissue repair. Interestingly, the swelling ratio and shape of the printed hydrogels were found to be preserved when immersed in a physiological environment. While DLP-printed hydrogels demonstrated impressive X- and Y-resolutions (85 µm), they were limited in producing hollow objects in the Z direction. To address this limitation, the 3D printing of complex mCMC hydrogels through Two-Photon Polymerization (TPP) was investigated for the first time, using a second formulation composed of 4 wt% mCMC (DM = 50 %). 3D scaffolds with cavities of 30 µm were successfully printed with a resolution of 10 µm, paving the way for the design of scaffolds with controlled and precise structures, for soft tissue engineering.

3D printing, carboxymethylcellulose, photo-crosslinking, hydrogel, scaffold, biomedical applications.

Acknowledgements

Financial support from the cross-cutting CEA program 'Matériaux et Procédés' is gratefully acknowledged (CelluloMed project). The authors acknowledge the Agence Nationale de la Recherche for financial support through the LabEx ARCANE program (ANR-11-LABX-0003-01) and the Graduate School of Chemistry, Biology and Health of University Grenoble Alpes CBH-EUR-GS (ANR-17-EURE-0003) and Glyco@Alps. The authors acknowledge the NanoBio chemistry platform (ICMG UAR 2607) for granting access to the electron microscopy facilities. The authors also acknowledge Ashland for kindly offering carboxymethylcellulose.

Conflicts of interest

All authors declare that they have no known competing financial interests or personal relationships that could have appeared to influence the work reported in this paper.

1. Introduction

Hydrogels are water-containing crosslinked polymer networks that have emerged as promising materials in biomedical applications due to their unique biocompatibility, tunable mechanical properties and ability to absorb and retain water [1]. In addition, these matrices closely mimic the physiological environment, making them ideal for drug delivery, tissue engineering and wound healing [2–5]. Indeed, their ability to encapsulate bioactive molecules and promote cell growth and tissue regeneration makes hydrogels essential for progress in biomedical research and clinical therapies [6].

However, one of the main challenges in the formation of hydrogels for medical applications lies in their often crude shaping and, therefore in the necessity to develop processing methods to faithfully reproduce the complexity of the human environment and tissues [7,8]. To this end, additive manufacturing is widely considered, as it enables the 3D printing of complex layered hydrogel structures from digital models [9–11]. Additive manufacturing processes have been successfully applied to shape hydrogels for medical applications, such as scaffolds for tissue engineering [12], biosensor systems [13] and tumor models for drug testing [14]. Two categories of additive manufacturing processes have been used to print hydrogels. The first category includes extrusion printing [15–17] and inkjet printing [9] technologies, requiring specific ink rheological properties and a robot-controlled print head. Another 3D printing categories called “vat polymerization” relies on the control of the print trajectory by light to initiate the photo-crosslinking of a liquid resin layer by layer, creating a 3D object. Vat polymerization includes several techniques such as Digital Light Processing (DLP) [18,19] and Two-Photon Polymerization (TPP or 2PP) [20]. DLP is based on the projection of a pattern of UV light onto the resin surface to crosslink the photosensitive resin selectively. TPP alternatively uses focused ultrashort laser pulses to induce polymerization at a precise focal point in the resin, enabling the construction of highly detailed and complex 3D structures [21].

In the case of 3D-printed hydrogels using vat polymerization techniques, the most widely studied polymers for biomedical applications are gelatin (a protein-based material) [22] or polyethylene glycol [23], previously functionalized with light-sensitive groups such as (meth)acrylates or norbornenes [7]. Similarly, polysaccharides are increasingly studied for hydrogel design due to their biocompatibility, biodegradability, natural abundance and their ability to be chemically modified to modulate their properties for specific applications [2,24]. In this context, photo-crosslinkable polysaccharides such as pullulan [25], hyaluronic acid (HA) [26,27], chitosan [28,29] or carboxymethylcellulose (CMC) [30,31] have been synthesized for 3D printing of hydrogels, but are still underutilized [32]. Using DLP, hydrogels with relatively poor resolutions in the X- and Y-directions were obtained from norbornene-modified HA (~100 µm) [27] or methacrylated CMC (> 500 µm) [30]. In any case, DLP seemed somewhat limited for the printing of hollow hydrogels due to the UV beam transmission through the hydrogel layers, even in the presence of a photoabsorber [30,31]. On the other hand, very interesting resolutions of ~5 µm and ~10 µm were obtained for TPP-printed hydrogels from UV-crosslinkable formulations based on methacrylated HA [26] and chitosan [28], respectively. Indeed, using inert visible light only leads to photo-crosslinking at the beam focal point, making TPP ideal for printing detailed hydrogel scaffolds.

In short, 3D printing of CMC-based hydrogels seemed quite limited using DLP and has never been tested using TPP yet. However, CMC is more affordable and more available than much of other polysaccharides. Moreover, its solubility in water and its numerous hydroxyl groups facilitate its chemical modification in aqueous media [33]. Consequently, the development of 3D-printable CMC-based hydrogels is of great interest for biomedical applications such as drug delivery [34] or tissue engineering [35].

In the present work, DLP and TPP technologies have been considered to print hydrogels with complex shapes from methacrylated CMC (mCMC) formulations. Both techniques were evaluated to particularly

design an hydrogel scaffold with appropriate dimensions to promote cell growth required for soft tissue repair [37].

2. Materials and methods

2.1. Materials

Methacrylic anhydride (MA) containing 2,000 ppm topanol A as inhibitor, 2-hydroxy-4′-(2-hydroxyethoxy)-2-methylpropiophenone (I2959 also known as Irgacure® 2959), deuterium oxide (D_2O), lithium phenyl-2,4,6-trimethylbenzoylphosphinate (LAP), phosphate-buffered salt solution (PBS, pH = 7.4), Bind-Silane (Methacryloxypropyltrimethoxysilane) and anhydrous sodium hydroxide pellets were purchased from Sigma Aldrich (France) and used as received. Sodium salt of CMC (NaCMC, reference BLANOSE 7LP EP, a kind gift from Ashland, France) with a weight-average molar mass of 90.5 $kg.mol^{-1}$ and a degree of substitution of 0.7 was also used as received.

2.2. Methacrylation of carboxymethylcellulose

Methacrylated carboxymethylcellulose (mCMC) was synthesized as previously reported [36]. NaCMC was solubilized at 2 wt% in deionized water at room temperature under mechanical stirring at 2,000 rpm, with an anchor-shaped glass pall. MA was then added dropwise to the CMC solution with molar ratios of 1.24 and 2.48 between MA and CMC hydroxyl groups (MA/OH). The reaction was continued for 2 h at room temperature. During the reaction, the pH was constantly adjusted to 8 with a 10 M NaOH solution. The resulting mixture was purified for 14 days by dialysis against deionized water using a cellulose mixed-ester membrane (MWCO = 12-14 kg/mol; Roth, Germany). Then, the mCMC product was freeze-dried for 5 days with a CHRIST Beta 2-8 LS plus lyophilizer (Martin Christ Gefriertrocknungsanlagen, Germany). Depending on the selected MA/OH ratio (1.24 or 2.48), mCMC with respective degrees of methacrylation (DM) of 34 ± 4 % or 50 ± 5 % were obtained, according to NMR measurements (Figure S1). Qualitative evaluation of the methacrylation was also performed by FT-IR spectroscopy (Figure S2).

2.3. Preparation and photo-crosslinking of aqueous mCMC formulations

The freeze-dried mCMC samples were dissolved at 2 or 4 wt% in deionized water at 50 °C, during 12h under magnetic stirring (Table 1). These concentrations were defined considering the mCMC solubility in water and the viscosity of the formulations [36]. Two different water-soluble and non-toxic photoinitators (PI) were used [38], depending on the considered 3D techniques, using a constant molar ratio compared to the number of moles of methacrylates (MA) in solution (nPI/nMA = 0.55). LAP absorbing at 385 nm, and I2959 absorbing at 266 nm, were chosen for DLP and TPP formulations, respectively. The considered photo-initiator was added after complete solubilisation of mCMC. The formulations were first placed in an ultrasound bath for 20 min, then under stirring during 12 h before printing. The influence of the concentrations and the DM of the considered mCMC on the properties of photo-crosslinked hydrogels have been discussed in a previous paper [36].

Table 1. Composition of the photo-crosslinkable mCMC formulations containing I2959 or LAP as photoinitiator.

Formulation	**mCMC**		**Photoinitiator**		**Water**	**3D technique**
	DM (%)	Concentration (wt%)	Name	Concentration (wt%)	Concentration (wt%)	
LAP-2	34 ± 4	2	LAP	0.15	97.85	DLP
IRG-4	50 ± 5	4	I2959	0.40	95.60	TPP

2.4. Hydrogel printing with Digital Light Processing (DLP)

Hydrogels were 3D-printed from the LAP-2 formulation using an Asiga MAX DLP printer (Asiga, Australia), having a UV light source emitting at 385 nm, and at an irradiance of 18 mW/cm². The Asiga MAX printer allows minimal theoretical resolutions of 62 µm (X- and Y-axes) and 1 µm (Z-axis), corresponding to the resolution of each projected pixel, and the height modulation of the build platform, respectively. Before printing, computer-aided design (CAD) models were drawn using the SolidWorks software (Dassault Systèmes, France), or directly upload from the Thingiverse database. The corresponding .STL file was then converted using the Composer software (Asiga, Australia). The structure of the objects was chosen to define the printing parameters and the maximum achievable resolutions.

For each printed part, the exposure time was 5 s for the first layer and 4 s for the subsequent layers. Circular hydrogels of 15 mm diameter and 4 mm thick (Model A), were first printed with layers of 100 (A1), 250 (A2), or 500 µm (A3). Other printed objects were: (Model B, Figure 2a) a four-stage pyramid with dimensions of 14 x 14 x 8 mm^3 (L x W x H) and a step height and width of 2 mm; (Model C, Figure 2b) a conical structure on a flat base, with dimensions of 19.82 x 10.48 x 9.75 mm^3 (L x W x H), and cones of 3 mm in height, on cylinder bases of 3 mm in diameter and 1 mm in height; (Model D, Figure 2c) a gear with external and internal diameters of 22.97 and 7.5 mm respectively, and a height of 11.00 mm; (Model E, Figure 2d) a flat grid with dimensions of 5.4 x 5.4 x 0.81 mm^3 (L x W x H), featuring 81 channels with diameter of 340 µm and wall thickness of 200 µm. The layer thickness was optimized depending on the objects to be printed, as discussed later.

The printed hydrogels were then rinsed with water and underwent UV post-curing for 3 minutes in a TwinCure UV tank (Medifive, South Korea), composed of a turntable surrounded by 7 dual-wavelength UV LEDs emitting at 365 nm and 405 nm, with an irradiance of 6 mW/cm². The effect of post-curing was studied through hydrogel characterization. The hydrogels were then captured using a Galaxy S20 FE smartphone (Samsung, South Korea) or a VHX-7000 digital microscope (Keyence, France). Finally, hydrogels were placed in an aluminum basket, filled with liquid nitrogen and freeze-dried overnight with the same lyophilizer to yield cryogels.

2.5. Hydrogel printing with Two-Photon Polymerization (TPP)

Hydrogel 3D-printing through TPP was carried out using the µFab3D.Advanced printer from Microlight 3D (France). It is equipped with an inverse microscope featuring an air lens with X20 magnification (Olympus, France) and a 0.8 NA numerical aperture. A 3D piezoelectric stage moving up to 300 µm along the X-, Y- and Z-axes, positions the focal point of the laser in a small volume (~1 $µm^3$) called a voxel. The µFab3D.Advanced laser generates green femtosecond pulses at λ = 532 nm with a maximum power of 20 mW. A maximum resolution of ~200 nm can be achieved depending on the printed material and conditions. The Luminis software (Microlight 3D, France) was used to design the objects to be printed.

Scaffolds shaped hydrogels (Model F, Figure 5a) with dimensions of 160 x 120 x 60 $µm^3$ (L x W x H) and well shaped hydrogels (Model G, Figure 5b) with dimensions of 50 x 50 x 50 $µm^3$ (L x W x H) were printed as described. First, a drop of mCMC-based formulation was placed on a clear glass slide, 24 mm square and 150-170 µm thick, pre-treated with Bind-Silane to enable the hydrogel adhesion to the slide. The latter was then fixed to the stage. For photo-crosslinking, the laser power was set to 4 mW and the printing speed to 187.5 $µm.s^{-1}$, inducing an exposure time of 2 s. With these parameters, the theoretical voxel height was 7 µm. Hydrogel images were first captured on the post-print TPP computer with the 0.8 NA x20 lens (Olympus, France). Residual formulation was removed by washing the sample for 1 minute in a PBS solution. Next, the hydrogel was post-cured with a UV lamp emitting at 274 nm (UV 701435, Jeulin, France), then dried under air or with an absorbent sheet. Post-development images of the printed hydrogels were taken using an optical microscope (Olympus, France) with x100

magnification, a Dino-lite (RS AM4815ZTL, Dino-lite, France) with x232.9 magnification, and a digital microscope without eyepiece (RYECOCAM, Switzerland).

2.6. Characterization techniques

2.6.1. ^{1}H NMR spectroscopy

^{1}H NMR spectroscopy was used to quantify the degree of methacrylation (DM) of the mCMC samples. 4.5 mg of mCMC was dissolved in 650 µL of D_2O at 50 °C for 12 h using a ThermoMixer C (Eppendorf, Germany). All ^{1}H NMR spectra were recorded on a Spectrospin 300 MHz spectrometer (Bruker, Germany) at 25 °C from 64 successive scans with a relaxation time D1 of 3 s.

2.6.2. Scanning electron microscopy (SEM)

SEM was used to investigate the cryogel morphology and measure the pore size distribution. Samples were fractured horizontally and pasted on metallic stubs with carbon cement, fractured and sputter-coated with Au/Pd. Secondary electron images were recorded with a FEI Quanta 250 (Thermo Fisher Scientific, US) scanning electron microscope equipped with a field emission gun operating at 2.5 kV. All pores were observed on the fractured surface. The pore size was determined by image treatment with the ImageJ software. Horizontal or vertical lines were drawn on each pore giving the average pore size. This procedure was performed on 25 pores per image and 4 images per sample. Pores whose walls were broken by the cutting method were not measured.

2.6.3. Swelling ratio

Swelling tests were performed on hydrogels printed by DLP in 250 µm layers and then further post-cured for 3 minutes, and on the corresponding cryogels. For each swelling experiment, three independent measurements were performed on three different samples. The samples were immersed in deionized water or in PBS at 37 °C in an oven. The swollen hydrogels or the rehydrated cryogels were regularly weighed. These steps were repeated until mass equilibrium was reached to determine the swelling ratio (SR) according to Eq. 1.

$$SR\ (t) = w_t / w_0 \qquad \text{Eq. 1}$$

where w_0 is the initial weight of the considered initial hydrogel or the corresponding cryogel, and w_t is the weight of the swollen hydrogel or the rehydrated cryogel at measurement time t.

2.6.4. Rheology measurement

All rheology measurements were performed using a Kinexus Pro+ parallel plate rheometer (Netzsch, Germany).

First, real-time rheology measurements were performed during UV photo-crosslinking, manually controlled using a UFIBER-COL UV fiber lamp 385 nm (UWAVE, France). The photo-crosslinkable mCMC-based formulations were deposited on a UV-transparent quartz plate. The mobile plane had a diameter of 20 mm and the gap between this plane and the quartz plate was 0.2 mm. The UV lamp was placed underneath the quartz plate at a distance allowing an exposure of 2 cm in diameter with an average power density of 18 $mW.cm^{-2}$. The elastic (G') and viscous (G") shear moduli were measured over time with a 5 % strain, at 0.1 Hz and at room temperature. After 1 minute of stabilization without UV irradiation, the radiation was turned on during 4 minutes. The experiments were carried out on three different samples.

Hydrogels printed with DLP were also characterized. Frequency sweep measurements were performed at a constant temperature (25 °C) from 0.1 to 10 Hz. According to preliminary amplitude sweep measurements, all tests were carried out in the linear viscoelastic region at 1 % strain. The gap between

the plate and the mobile plane (20 mm diameter) was set to 0.6 mm. All the experiments were carried out on three different samples.

3. Results and discussion

3.1. Evaluation of photo-crosslinking kinetics of CMC-based hydrogel for DLP printing

The LAP-2 formulation containing 2 wt% of mCMC with a DM of 34%, and 0.15 wt% of LAP (Table 1), was evaluated for the 3D printing of hydrogels using DLP. This formulation was selected because its low viscosity makes it suitable for DLP additive manufacturing [39]. Given that LAP has no toxic effect [38], the LAP-2 formulation is expected to lead to biocompatible hydrogels. Indeed, previous hydrogels obtained with the same mCMC composition and with Irgacure 2959 as photoinitiator were proved to be non-cytotoxic [40].

The photo-crosslinking kinetics of this formulation was first characterized by real-time rheology to provide essential information about the exposure time required using vat polymerization techniques (Figure 1a). In these experiments, after 60 s of stabilization of the elastic (G') and viscous (G") shear moduli, the application of UV light led to a progressive increase of both G’ and G” values until reaching a solid-like behavior (G’ > G”). Considering the intersection between the G' and G" curves, a gelation time of 2.7 ± 0.10 s seconds was measured for the LAP-2 formulation, in good agreement with Melilli *et al.* who reported a 2 s gelation time for an equivalent formulation containing 2 wt% mCMC with a DM of 60 % [30]. It is well established that for UV-curable resins used in vat polymerization techniques, the insolation time for each layer must be at least equal to the gelation time in order for the layer to be rigid enough to be selfstanding [41]. Knowing that, and after printing optimization of each layer, the exposure duration for the first layer of each printed part was set at 5 seconds to achieve a hydrogel rigid enough to adhere to the platform during printing and capable of supporting the final structure after removal from the build platform. For the subsequent layers, the exposure duration was set at 4 seconds, corresponding to the minimum duration to prevent the collapse of the printed structure.

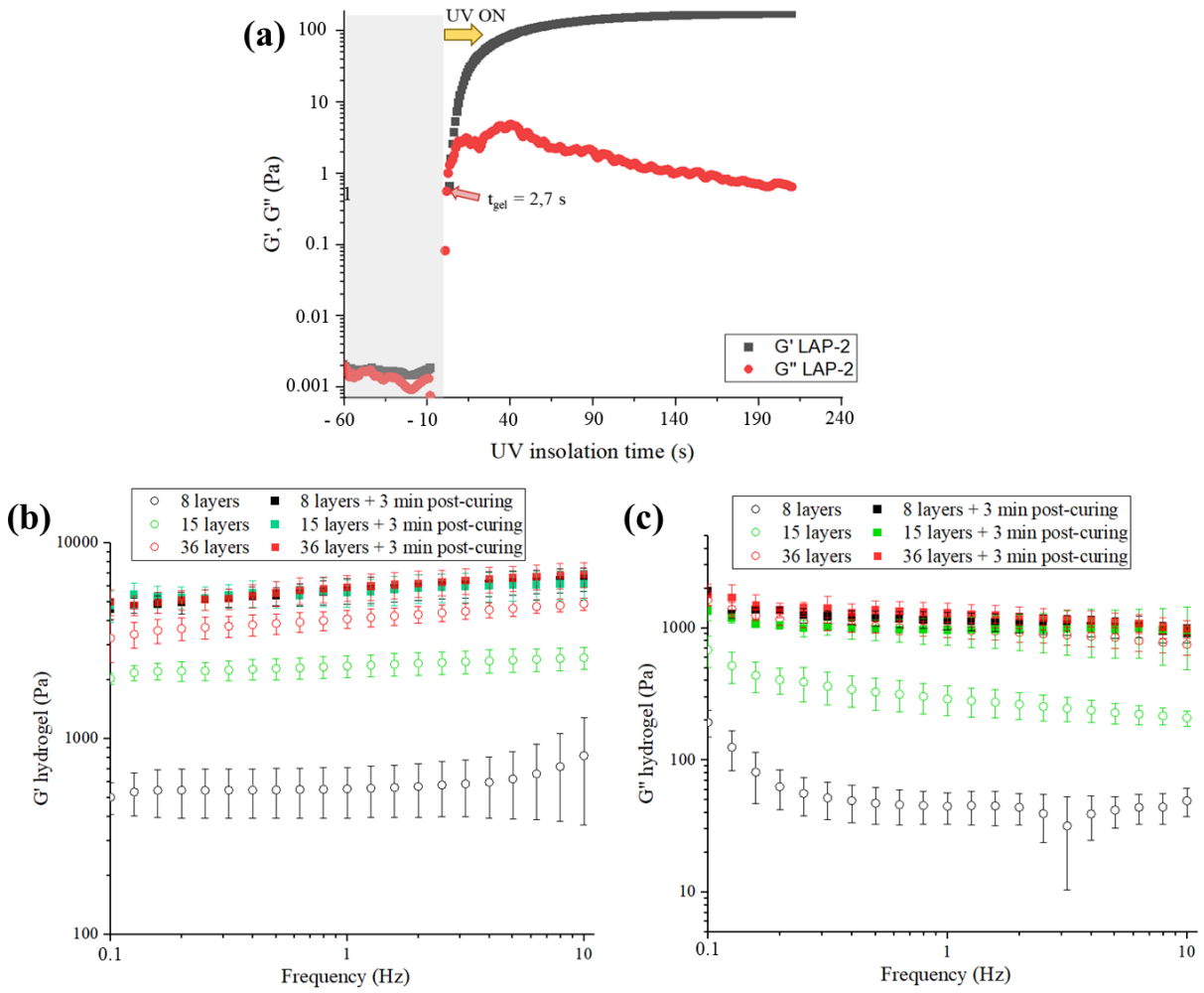

Figure 1. **(a)** Evolution of the elastic (G') and viscous (G'') shear moduli with the insolation time under UV light (385 nm) during real-time rheology measurements, for the LAP-2 formulation containing 2 wt% mCMC with a DM of 34 %, and 0.15 wt% LAP. Elastic (G') **(b)** and viscous (G") **(c)** shear moduli measured between 0.1 and 10 Hz and at 1% strain at 25 °C, for 4 mm-thick hydrogels printed from the LAP-2 formulation. Exposure times were 5 s for the first layer and 4 s for subsequent layers. Thicknesses were 500 µm for the first layer and 100 µm (36 layers, A1), 250 µm (15 layers, A2) and 500 µm (8 layers, A3) for subsequent layers. Measurements were performed before and after a 3 min UV post-curing (365 nm + 405 nm, 6 mW.cm^{-2}).

Using these exposure durations, cylindrical hydrogels (Model A) were printed using layer thicknesses of 100 µm (A1), 250 µm (A2) or 500 µm (A3). Considering the total thickness of 4 mm for the hydrogels and a constant thickness of 500 µm for the first layer, the number of printed layers was 36, 15 or 8, respectively. The viscoelastic properties of all cylindrical hydrogels as printed (A1, A2, A3) and after post-curing (A1C, A2C, A3C) was then investigated, to evaluate the time required for maximum crosslinking (Figure 1, Supporting information Figure S3). First, for all studied hydrogels, the elastic shear modulus (G') was always higher than the viscous shear modulus (G'') over the studied frequency range (0.1-10 Hz), reflecting the predominantly solid-elastic behavior of hydrogels. Very interestingly, for as printed hydrogels before post-curing, the G' and G'' moduli increased with the number of printed layers (Figure b,c). For example, at 1 Hz, G' moduli of 550 ± 160 Pa, 2400 ± 310 Pa and 4100 ± 440 Pa and G'' moduli of 45 ± 12 Pa, 290 ± 74 Pa and 980 ± 130 Pa, were measured for hydrogels A3, A2 and A1 consisting of 8, 15 and 36 layers, respectively. This could be explained by differences in total insolation time and, therefore, in the crosslinking density of the hydrogels. As an example, at the end of the hydrogel printing, the total insolation time of the first layers was estimated to 33 s, 61 s and 145 s, for hydrogels A3, A2 and A1, respectively. The viscoelastic properties of all hydrogels were also measured after post-curing. It was observed that a post-curing of 3 minutes at 6 mW.cm^{-2} was sufficient

to complete crosslinking. Indeed, this post-curing duration allowed to reach maximum G' and G'' moduli, regardless of the number of printed layers. Indeed, at 1 Hz, hydrogels A1C, A2C and A3C showed G' moduli of 5900 ± 910 Pa, 5600 ± 890 Pa and 5200 ± 47 Pa, and G'' moduli of 1300 ± 240 Pa, 960 ± 230 Pa and 1100 ± 170 Pa, respectively. These non-significant differences in G' and G'' values indicated that the final viscoelastic properties of the post-cured hydrogels did not depend on the number of printed layers. It seems worth mentioning that the final viscoelastic properties of the post-cured hydrogels correspond to the ones of soft tissues, such as brain, liver or bone marrow [42]. These 3D-printed hydrogels could then be considered as extracellular matrix (ECM) for soft tissue repair. The following sections describe only A2 hydrogels printed with 15 layers and post-cured for 3 minutes.

3.2. Evaluation of DLP for the printing of mCMC hydrogels and cryogels with complex shapes

Other hydrogels with more complex shapes were printed from the LAP-2 formulation, to evaluate the resolution of DLP with such water-based resins. In additive manufacturing, resolution in the X- and Y-directions refers to the horizontal print quality of each layer and is determined by the fineness of detail that the 3D printer can reproduce on the surface of the printed objects [10]. In DLP specifically, the Z-resolution depends on the vertical modulation of the build platform, *i.e.* the thickness of each layer, but also on the exposure time.

The first complex shape studied was a four-stage pyramid (Model B), each stage being 2 mm in height (Z), with corresponding sides measuring 14 mm, 10 mm, 6 mm, and 2 mm (Figure 2a). This pyramid served as the primary model to first investigate the impact of the printed layer thickness and the exposure times on the print quality of hydrogels in the X- and Y-dimensions. Based on these experiments, the optimal thickness was set to 500 µm for each layer, while the exposure times were set at 5 s for the first layer, and 4 s for the subsequent layers (Figure 2e). This configuration prevented the hydrogel collapse and undesirable peripheral crosslinking that could impact the resolution of the printed part. Indeed, longer exposure times and lower layer thicknesses both led to peripheral crosslinking, due to the high diffusion of UV light through the different layers previously printed, mainly composed of water (Table S1, Figure S4). Consequently, DLP has exhibited important limitations in terms of layer thickness, and thus of Z-resolution, as the minimal printable thickness was between 250 and 500 µm, for such hydrogels composed of successive identical layers.

Conical hydrogels (Model C) were then printed to determine the highest achievable X- and Y-resolutions, while avoiding the printing of successive identical layers, thus mitigating the peripheral crosslinking phenomenon (Figure 2b). Layer thickness, set to 500 µm, 200 µm, 100 µm or 50 µm, directly influenced the final resolution of the printed hydrogels (Figure S5). With a layer thickness of 50 µm, the last crosslinked layer of the tip had a surface diameter of 85 ± 3 µm (Figures 2f, S5d). This value was slightly higher than the theoretical insolated diameter for this final layer, *i.e.* the size of a DLP pixel (62 µm), indicating a slight collapse of the tip. Nevertheless, DLP seemed quite suitable for the printing of hydrogels with conical shapes and interesting resolutions, and could be of interest for the 3D printing of rigid hydrogel microneedles in future work.

The present paper mainly focuses on the 3D printing of hydrogels scaffolds for cell growth, with multiple cavities of controlled dimensions to yield porous materials. In this context, two other complex shapes were printed using DLP. First, a gear with a 7.5 mm hole was printed to verify if such hollow hydrogels could be 3D-printed without collapsing (Model D, Figure 2c). The hole was printed in the Z-direction, and the resulting hydrogel conformed to the model and did not collapse (Figure 2g). Nevertheless, a modification of the hole was noticed, with an inner diameter ranging from 6.7 mm for the first layers, to 7.5 mm for the last layers, due to undesirable peripheral crosslinking. Similarly, small flat grids were printed to determine the minimum achievable hole diameter and wall thickness (Model E, Figure 2d). The smallest dimensions achieved without hydrogel collapse and without apparent peripheral crosslinking in the holes, were 340 µm for the inner channel diameter and 200 µm for the walls of the printed hydrogel (Figure 2h). Interestingly, the obtained channel dimensions correspond to

the pore sizes needed for the growth of most cells (100 – 200 µm). However, the printed hydrogel was not robust enough, and deteriorated during its removal from the platform.

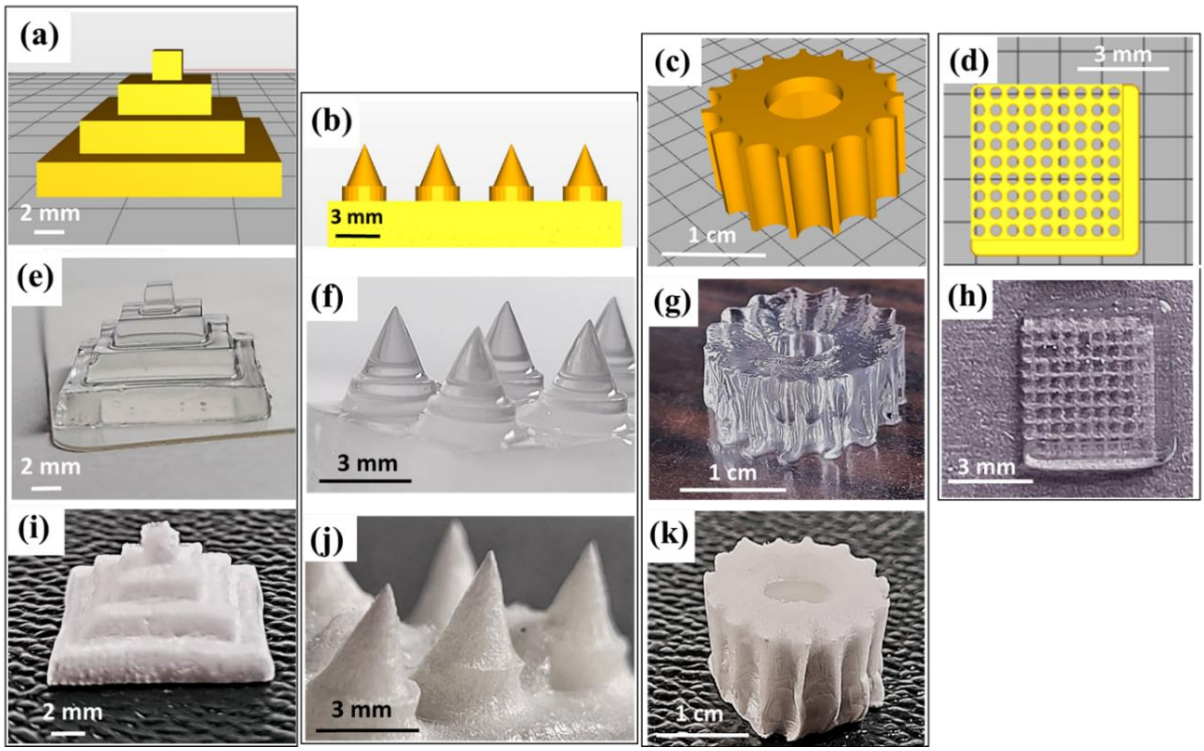

Figure 2. CAD models of **(a)** a pyramid structure with dimensions of 14 x 14 x 8 mm^3 (L x W x H, model B), **(b)** a conical structure on a flat base with dimensions of 19.82 x 10.48 x 9.75 mm^3 (L x W x H, model C), **(c)** a gear with an external diameter of 22.97 mm and a height of 11.00 mm (Model D), and **(d)** a flat grid of dimensions 5.4 x 5.4 x 0.81 mm^3 (L x W x H), with 81 channels of 340 µm diameter and wall thicknesses of 200 µm (Model E). **(e-h)** Corresponding hydrogels printed by DLP from the LAP-2 formulation containing 2 wt% mCMC with a DM of 34 % and 0.15 wt% LAP, with exposure times of 5 s for the first layer, then 4 s for subsequent layers, and with layer thicknesses of 500 µm (e,g,h) or 50 µm (f) and **(i-k)** corresponding freeze-dried cryogels.

Mellili *et al.* printed hydrogels with an identical DLP Asiga Max, from an aqueous formulation containing 2 wt% mCMC with a DM of 60 %, and 0.04 wt% LAP as photoinitiator [30]. In their work, the layer thickness was set to 50 µm, and the exposure time was not mentioned. Printed hydrogels had a X,Y resolution of over 500 µm, due to layer over insolation. In contrast, in the present work, the resolution obtained for printed mCMC hydrogels (85 µm) was comparable to those obtained by DLP for hydrogels composed of thiol-norbornene HA (100 µm) [27] or methacrylated chitosan (50 µm) [29]. Nevertheless, as observed by Mellili *et al.*, the challenge lies in the ability to print hydrogels with cavities along the Z-axis direction, from a formulation mainly composed of water [30]. Indeed, without the addition of a photoabsorber, the UV beam spreads across the entire formulation and initiates polymerization in the normally vacant areas (Figure S6). Adding a photoabsorber could be considered to enhance the Z-axis resolution and the complexity of the DLP-printed hydrogels, by reducing the depth of UV penetration into the resin. Nevertheless, conventional water-soluble photoabsorbers that absorb within the intended wavelength range, such as certain food dyes like tartrazine, are either toxic or suspected to be so [43,44]. As a result, these photoabsorbers are not desirable for medical applications, where biocompatible photoabsorbers should be preferred. In this context, Mellili *et al.* replaced the water in their mCMC formulation with a cell culture medium absorbing at 385 nm [30]. This strategy enabled the printing of hollow hydrogels with improved resolution but with lower mechanical strength. In summary, without the use of a cytotoxic photoabsorber, the 3D printing of a hydrogel scaffold with a complex structure consisting of holes and thin walls and exhibiting sufficient mechanical properties to be used in tissue engineering was not achievable from mCMC formulations using DLP. However, it is

necessary to emphasize that these mCMC formulations developed for DLP printing could still have interesting biomedical applications, such as the 3D printing of innovative microneedles.

Interestingly, the macroscopic structure of the printed hydrogels was retained during the freeze-drying process (Figure 2i-k). However, a slight vertical expansion of the cryogels was observed. For example, for the conical cryogels (C), increase of 300 µm in height corresponding to 10 % of the initial height of the tips, was noticed (Figure 2j). This vertical expansion was attributed to the freezing process with liquid nitrogen from bottom to top, aligning the pores along the vertical axis [36]. This phenomenon should be considered when designing hydrogel models. Furthermore, the average pore size observed by SEM for the cryogels was 25.5 ± 8.8 µm (Figure 3 a,b). This average pore size was not suitable for developing materials targeting cell growth and tissue repair, that should display pores around 100-200 µm [37,45]. Consequently, the preparation of cryogels through DLP-printed hydrogel freeze-drying did not seem an appropriate process for creating porous materials for tissue engineering.

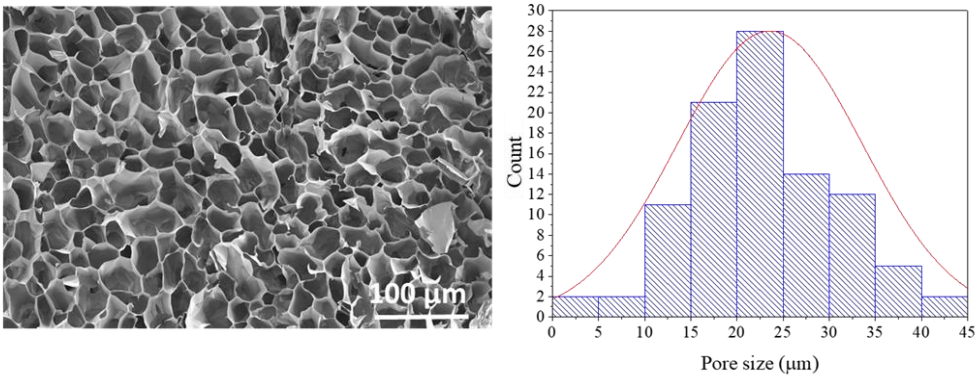

Figure 3. SEM images displaying the cryogel morphologies and corresponding pore size distributions for the cryogel printed from the LAP-2 formulation, with 250 µm layers exposed for 4 s (500 µm and 5 s for the first layer, A2). The average pore size was determined from 25 measurements on 4 images per sample. Pores whose walls were broken by the cutting section method were not considered.

3.3. Swelling properties of DLP-printed hydrogels and freeze-dried cryogels in physiological environment

Swelling ratios (SR), reflecting the capacity of a 3D polymer network to absorb and retain a specific fluid without breaking, were measured for the printed A2 cylinders, in the form of post-cured hydrogels, or after freeze-drying. Swelling was conducted in PBS at 37 °C to reproduce the saline conditions of the physiological environment. The experiments were carried out over several days to approach the conditions of use of hydrogels in implantable biomedical applications. First, the evolution of the SR of the hydrogel placed in PBS was monitored and compared to that in deionized water (Figure 4a). Interestingly, throughout the entire duration of the experiment, the hydrogel swelling in water was more important than in PBS. In both cases, swelling equilibria were reached few minutes after the introduction of the hydrogels into their respective environments. On the one hand, the SR in water was of 2.02 ± 0.110 at the equilibrium. When immersed in water, the mCMC chains of the printed hydrogel attracted and retained water molecules through hydrophilic interactions. This led to a significant swelling of the hydrogel, and to a twofold increase of the hydrogel volume, impacting the initial 3D shape printed with DLP. On the other hand, the SR in PBS was only of 1.06 ± 0.040. Very interestingly, the printed hydrogels did not significantly swell under saline conditions, thus retaining their initial printed shape. This swelling difference may be explained by the charge screening resulting from the high ionic strength of the PBS saline environment, limiting mCMC network stretching and, hence swelling. Furthermore, an osmotic equilibrium will occur upon introducing the hydrogel filled with pure water in the PBS medium [46]. Consequently, it seems unnecessary to consider any shape changes in the hydrogels when designing the numerical model for printing. Finally, the rheological properties of the swollen hydrogels at equilibrium in PBS at 37 °C were also compared to the ones of the initial hydrogels (Figure 4b). No

significant difference was observed between the elastic moduli (G'). For example, at 1 Hz, G' moduli of 5.6 ± 0.89 kPa and 5.2 ± 0.085 kPa were measured for the hydrogel before and after swelling in PBS, respectively. Small differences between post-cured hydrogels and PBS-swollen hydrogels were only measured at higher frequencies for the viscous shear moduli (G''). Indeed, at 10 Hz for example, G'' moduli of 0.96 ± 0.47 kPa and 1.7 ± 0.092 kPa were measured for the hydrogel before and after swelling in PBS, respectively. It can be concluded that the mCMC hydrogels printed with DLP maintain their shape and their viscoelastic properties when placed in a saline environment such as PBS at 37 °C. These results are crucial when considering these hydrogels for applications such as biological tissue repair or controlled drug delivery. To preserve the printed hydrogel prior to its application, freeze-drying may be necessary, due to the greater stability and mechanical properties of cryogels [36]. Thus, swelling of the cylindrical cryogels in PBS was also investigated (Figure S7). Equilibrium was reached after 24 hours with a SR of 33.9 ± 0.52. Interestingly, no difference was noted between the SR of hydrogels and cryogels in PBS. Indeed, the mass ratio between the swollen hydrogel and the cryogel was 33.8 ± 0.47, while it was 33.9 ± 0.52 between the rehydrated cryogel and the cryogel. Consequently, the freeze-drying step, allowing a better conservation of the printed hydrogels, did not modify the swelling properties of the materials in PBS.

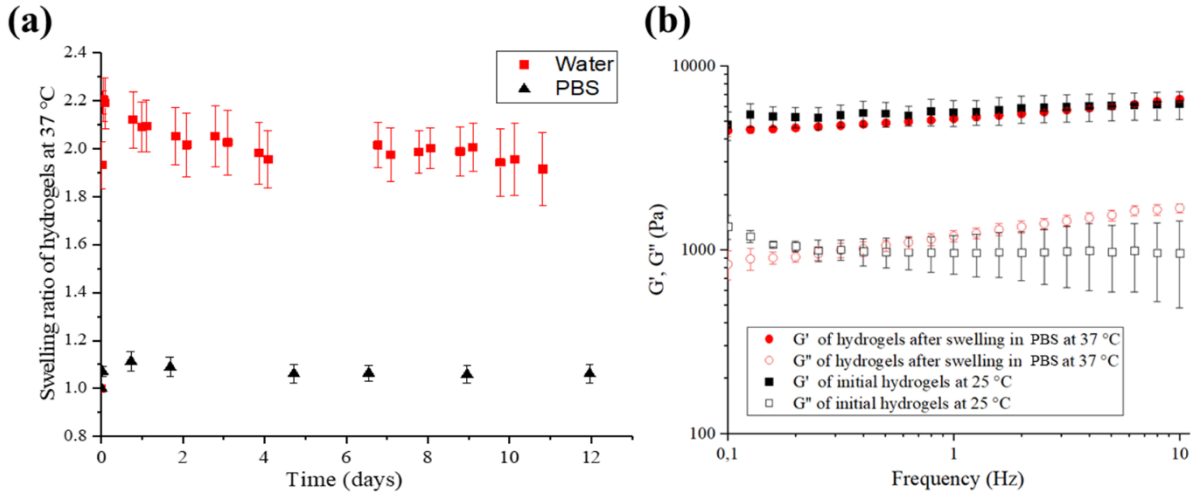

Figure 4. (a) Evolution of the swelling ratio of A2 hydrogels with time upon immersion in water or PBS at 37 °C. **(b)** Evolution of the elastic (G') and viscous (G'') shear moduli of the A2 hydrogels before and after swelling in PBS at 37 °C, measured by planar rheology from 0.1 to 10 Hz, at 1% strain. A2 hydrogels were printed with 250 µm layers exposed for 4 s (500 µm and 5 s for the first layer) from the LAP-2 formulation containing a concentration of 2 wt% mCMC with a DM of 34 % and 0.15 wt% LAP, then post-cured for 3 min.

3.4. Evaluation of TPP for the 3D printing of mCMC hydrogel scaffolds

Given that DLP was not suitable enough for the 3D printing of hydrogel scaffolds and that the pores of the corresponding cryogels were too small to allow cell growth, TPP was considered as an alternative vat polymerization technique for scaffold printing. To that end, the IRG-4 formulation containing 4 wt% of mCMC with a DM of 50 ± 5 % and 0.4 wt% of the I2959 photoinitiator, was developed to maximize the methacrylate concentration, and to initiate the photo-crosslinking at 266 nm (Table 1), based on preliminary tests (Table S2). Two objects representing a scaffold (Model F) and a well (Model G) were designed to define the printing parameters and to evaluate the resolution that could be achieved for mechanically stable hydrogels (Figure 5 a,b). Like scaffolds, wells could find various applications in the biomedical field, such as the encapsulation of cells or the vectorization of specific particles.

Using a laser power of 4 mW and a printing speed of 187.5 µm.s^{-1}, the hydrogels printed from the IRG-4 formulation, exhibited well-defined shapes without any noticeable defects, despite a slight edge effect around the well (Figure 5 c,d). However, the subsequent development of the hydrogels, involving hydrogel recovery and the removal of uncrosslinked formulation, proved to be quite challenging. First, the washing step was conducted with PBS to prevent hydrogel swelling and maintain its mechanical

properties and structural stability. Subsequent air-drying of the residual PBS led to the dehydration of the small-sized hydrogels, causing them to collapse (Figure S8). To counteract this phenomenon, the objects were rehydrated with PBS following dehydration. Nonetheless, during the drying process, additional intermolecular bonds, such as hydrogen bonds, ionic bonds, or hydrophobic interactions, may form between the mCMC chains. These new bonds can irreversibly alter the hydrogel structure, complicating the restoration of the hydrogel to its initial form upon rehydration with PBS. To prevent hydrogel dehydration during PBS drying, an alternate procedure involving the delicate removal of excess PBS with absorbent paper, while avoiding dehydration, was considered. This method required careful attention, yet effectively preserved the printed structure after development (Figure 5 e,f). Nevertheless, the characterization of such small-sized hydrogels was also challenging. Indeed, the microscopes used for the optical characterization of the printed hydrogels did not allow tilting the substrate, and therefore, did not allow clear visualization of the 3D structure. Moreover, given that these hydrogels comprised 95.6 wt% water, they were nearly transparent, explaining the poor quality of the images. To delve deeper into the optical characterization of the printed structures, it might be interesting to optimize the freeze-drying or the supercritical CO_2 drying of small-sized hydrogels. However, technical challenges such as transporting the hydrogels without alteration and drying them without modifying the microstructure or causing fracture need to be overcome and are currently under development.

After washing with this final procedure, the hydrogels printed using TPP exhibited cavities of approximately 30 µm in size for the scaffold (Model F) and 60 µm for the well (Model G), aligning with the dimensions of the CAD models. For the scaffold, the wall thickness of 10 µm was in the range of resolutions achieved for hydrogels printed from photo-crosslinkable HA-, pullulan- (5 µm) or chitosan-based formulations (10 µm) using TPP [26,28,47]. Consequently, TPP could be used for printing hydrogel scaffolds with high resolution and complex shapes from mCMC formulations. Due to the higher natural abundance of cellulose compared to other polysaccharides, mCMC-based hydrogels are expected to have easier adoption in the biomedical sector. However, considering that most tissue cells are on the scale of hundreds of micrometers, future work will have to optimize the model structures in order to approach an ideal scaffold for cell growth or cell encapsulation [37].

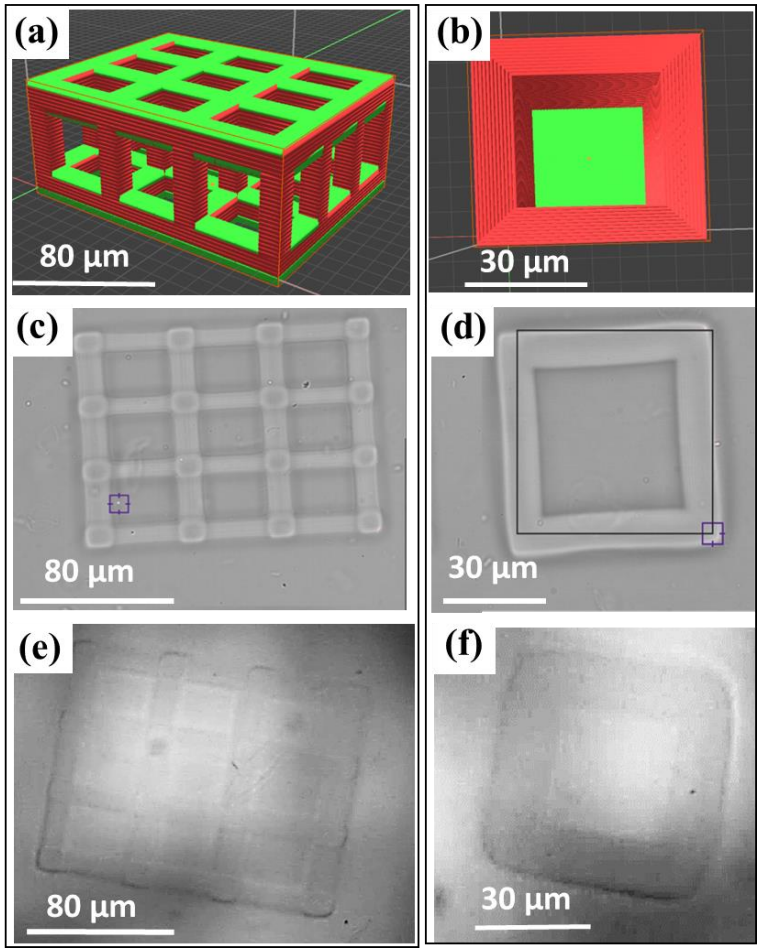

Figure 5. CAD models of **(a)** a scaffold with dimensions of 160 x 120 x 60 μm^3 (L x W x H, model F), and **(b)** a well with dimensions of 50 x 50 x 50 μm^3 (L x W x H, model G). Corresponding hydrogels printed by TPP from the IRG-4 formulation containing 4 wt% mCMC with a DM of 50% and 0.4 wt% I2959, using a 4 mW laser beam at a speed of 187.5 $\mu m.s^{-1}$, and observed directly after printing **(c,d)** and after development by drying with absorbent paper **(e,f)**. As-printed hydrogels were observed using an inverse microscope featuring an air lens with X20 magnification and a 0.8 NA (Olympus, France), while developed hydrogels were characterized with a Dino-lite with x232.9 magnification (Dino-lite, France).

4. Conclusion

Two distinct photo-crosslinkable aqueous formulations were developed from methacrylated carboxymethylcellulose (mCMC) to investigate their printability using two vat polymerization techniques, namely Digital Light Processing (DLP) and Two-Photon Polymerization (TPP), for manufacturing innovative hydrogels with complex shapes for biomedical applications. After defining the photo-crosslinking kinetics of the LAP-2 formulation containing 2 wt% mCMC with a degree of methacrylation (DM) of 34%, through real-time rheology characterization, the printing conditions of hydrogels using DLP were optimized in terms of layer thickness as well as insolation and post-curing times. The final hydrogels showed viscoelastic properties like the ones of human soft tissues, such as liver, brain, and bone marrow, with elastic and viscous shear moduli of 5.6 ± 0.4 kPa and 1.1 ± 0.2 kPa, respectively. Consequently, such 3D-printed hydrogels could be considered as extracellular matrix for soft tissue repair. The swelling properties of printed hydrogels were also investigated. Interestingly, after being introduced into a phosphate-buffered solution (PBS) at 37 °C to simulate the salinity of the physiological environment, the hydrogels maintained their structure without significant swelling, thus preserving their viscoelastic properties. Moreover, freeze-dried cryogels immersed in PBS regained a swelling ratio comparable to that of the initial hydrogel, reabsorbing a similar amount of PBS. This

indicates that freeze-drying could be used for improved conservation and transportation of the hydrogel. Nevertheless, printing assays showed that the printable hydrogel geometries are quite limited using DLP and the LAP-2 formulation. Indeed, peripheral polymerization was observed when printing successive layers with the same surface. Consequently, DLP was found to be more suitable for the 3D printing of conical hydrogels, with X- and Y-resolutions of 85 µm and could be considered for the manufacturing of rigid hydrogel microneedles for drug administration or biological fluid sampling. Nevertheless, due to the preponderance of water in the photo-crosslinkable formulation (97.85 wt%), the Z-resolution was found to be insufficient to print hydrogels with cavities perpendicular to the Z-axis, preventing the use of DLP for the 3D printing of scaffolds for tissue engineering, without the use of water-soluble but toxic photo-absorber. Finally, TPP was considered as an alternative vat polymerization method to print small-sized hydrogels with complex shapes and high resolutions from mCMC aqueous formulations.

The IRG-4 formulation, consisting in 4 wt% of mCMC with a DM of 50% and of 0.4 wt% of I2959 diluted in water, was especially developed for maximizing the number of photo-crosslinkable groups, and to be printable with the Microlight 3D apparatus. A development procedure for recovering the printed hydrogels and removing the excess of uncrosslinked formulation was developed. Hydrogel scaffolds and well structures with resolutions of 10 µm were successfully obtained, paving the way for the design of scaffolds with controlled and precise spatial arrangement for soft tissue engineering.

Data availability

All relevant data are included in the manuscript as Source Data or Supplementary information. All other data are available from the corresponding authors upon reasonable request.

References

[1] S.H. Aswathy, U. Narendrakumar, I. Manjubala, Commercial hydrogels for biomedical applications, Heliyon 6 (2020) e03719. https://doi.org/10.1016/j.heliyon.2020.e03719.

[2] R. Barbucci, ed., Hydrogels: biological properties and applications, Springer, Milan ; New York, 2009.

[3] T.R. Hoare, D.S. Kohane, Hydrogels in drug delivery: Progress and challenges, Polymer 49 (2008) 1993–2007. https://doi.org/10.1016/j.polymer.2008.01.027.

[4] F. Fan, S. Saha, D. Hanjaya-Putra, Biomimetic Hydrogels to Promote Wound Healing, Front. Bioeng. Biotechnol. 9 (2021) 718377. https://doi.org/10.3389/fbioe.2021.718377.

[5] X. Bai, M. Gao, S. Syed, J. Zhuang, X. Xu, X.-Q. Zhang, Bioactive hydrogels for bone regeneration, Bioact. Mater. 3 (2018) 401–417. https://doi.org/10.1016/j.bioactmat.2018.05.006.

[6] H. Chamkouri, A Review of Hydrogels, Their Properties and Applications in Medicine, Am. J. Biomed. Sci. Res. 11 (2021) 485–493. https://doi.org/10.34297/AJBSR.2021.11.001682.

[7] J. Li, C. Wu, P.K. Chu, M. Gelinsky, 3D printing of hydrogels: Rational design strategies and emerging biomedical applications, Mater. Sci. Eng. R Rep. 140 (2020) 100543. https://doi.org/10.1016/j.mser.2020.100543.

[8] S. Kholgh Eshkalak, E. Rezvani Ghomi, Y. Dai, D. Choudhury, S. Ramakrishna, The role of three-dimensional printing in healthcare and medicine, Mater. Des. 194 (2020) 108940. https://doi.org/10.1016/j.matdes.2020.108940.

[9] H. Quan, T. Zhang, H. Xu, S. Luo, J. Nie, X. Zhu, Photo-curing 3D printing technique and its challenges, Bioact. Mater. 5 (2020) 110–115. https://doi.org/10.1016/j.bioactmat.2019.12.003.

[10] M. Pagac, J. Hajnys, Q.-P. Ma, L. Jancar, J. Jansa, P. Stefek, J. Mesicek, A Review of Vat Photopolymerization Technology: Materials, Applications, Challenges, and Future Trends of 3D Printing, Polymers 13 (2021) 598. https://doi.org/10.3390/polym13040598.

[11] L.R.R. da Silva, W.F. Sales, F. dos A.R. Campos, J.A.G. de Sousa, R. Davis, A. Singh, R.T. Coelho, B. Borgohain, A comprehensive review on additive manufacturing of medical devices, Prog. Addit. Manuf. 6 (2021) 517–553. https://doi.org/10.1007/s40964-021-00188-0.

[12] R. Cruz-Medina, D.A. Ayala-Hernández, A. Vega-Rios, E.I. López-Martínez, M.E. Mendoza-Duarte, A. Estrada-Monje, E.A. Zaragoza-Contreras, Curing of Cellulose Hydrogels by UV

Radiation for Mechanical Reinforcement, Polymers 13 (2021) 2342. https://doi.org/10.3390/polym13142342.
[13] R. Anastasio, W. Peerbooms, R. Cardinaels, L.C.A. van Breemen, Characterization of Ultraviolet-Cured Methacrylate Networks: From Photopolymerization to Ultimate Mechanical Properties, Macromolecules 52 (2019) 9220–9231. https://doi.org/10.1021/acs.macromol.9b01439.
[14] V.G. Muir, J.A. Burdick, Chemically Modified Biopolymers for the Formation of Biomedical Hydrogels, Chem. Rev. (2020) acs.chemrev.0c00923. https://doi.org/10.1021/acs.chemrev.0c00923.
[15] G. Tejada Jacob, V.E. Passamai, S. Katz, G.R. Castro, V. Alvarez, Hydrogels for extrusion-based bioprinting: General considerations, Bioprinting 27 (2022) e00212. https://doi.org/10.1016/j.bprint.2022.e00212.
[16] C.M.S. Vicente, M. Sardinha, L. Reis, A. Ribeiro, M. Leite, Large-format additive manufacturing of polymer extrusion-based deposition systems: review and applications, Prog. Addit. Manuf. 8 (2023) 1257–1280. https://doi.org/10.1007/s40964-023-00397-9.
[17] K.S. Pandya, S.S. Shindalkar, B. Kandasubramanian, Breakthrough to the pragmatic evolution of direct ink writing: progression, challenges, and future, Prog. Addit. Manuf. 8 (2023) 1303–1328. https://doi.org/10.1007/s40964-023-00399-7.
[18] R. Chaudhary, P. Fabbri, E. Leoni, F. Mazzanti, R. Akbari, C. Antonini, Additive manufacturing by digital light processing: a review, Prog. Addit. Manuf. 8 (2023) 331–351. https://doi.org/10.1007/s40964-022-00336-0.
[19] J. Zhang, Q. Hu, S. Wang, J. Tao, M. Gou, Digital Light Processing Based Three-dimensional Printing for Medical Applications, Int. J. Bioprinting 6 (2019) 1. https://doi.org/10.18063/ijb.v6i1.242.
[20] X. Jing, H. Fu, B. Yu, M. Sun, L. Wang, Two-photon polymerization for 3D biomedical scaffolds: Overview and updates, Front. Bioeng. Biotechnol. 10 (2022) 994355. https://doi.org/10.3389/fbioe.2022.994355.
[21] Z. Faraji Rad, P.D. Prewett, G.J. Davies, High-resolution two-photon polymerization: the most versatile technique for the fabrication of microneedle arrays, Microsyst. Nanoeng. 7 (2021) 71. https://doi.org/10.1038/s41378-021-00298-3.
[22] W. Ye, H. Li, K. Yu, C. Xie, P. Wang, Y. Zheng, P. Zhang, J. Xiu, Y. Yang, F. Zhang, Y. He, Q. Gao, 3D printing of gelatin methacrylate-based nerve guidance conduits with multiple channels, Mater. Des. 192 (2020) 108757. https://doi.org/10.1016/j.matdes.2020.108757.
[23] M.A. Sarabia-Vallejos, F.E. Cerda-Iglesias, C.A. Terraza, N.A. Cohn-Inostroza, A. Utrera, M. Estrada, J. Rodríguez-Hernández, C.M. González-Henríquez, Biocompatible and bioactive PEG-Based resin development for additive manufacturing of hierarchical porous bone scaffolds, Mater. Des. 234 (2023) 112315. https://doi.org/10.1016/j.matdes.2023.112315.
[24] A. Kirschning, N. Dibbert, G. Dräger, Chemical Functionalization of Polysaccharides-Towards Biocompatible Hydrogels for Biomedical Applications, Chem. - Eur. J. 24 (2018) 1231–1240. https://doi.org/10.1002/chem.201701906.
[25] Z. Feng, J. Li, D. Zhou, H. Song, J. Lv, W. Bai, A novel photocurable pullulan-based bioink for digital light processing 3D printing, Int. J. Bioprinting 9 (2022). https://doi.org/10.18063/ijb.v9i2.657.
[26] O. Kufelt, A. El-Tamer, C. Sehring, S. Schlie-Wolter, B.N. Chichkov, Hyaluronic Acid Based Materials for Scaffolding via Two-Photon Polymerization, Biomacromolecules 15 (2014) 650–659. https://doi.org/10.1021/bm401712q.
[27] J.H. Galarraga, A.P. Dhand, B.P. Enzmann, J.A. Burdick, Synthesis, Characterization, and Digital Light Processing of a Hydrolytically Degradable Hyaluronic Acid Hydrogel, Biomacromolecules 24 (2023) 413–425. https://doi.org/10.1021/acs.biomac.2c01218.
[28] O. Kufelt, A. El-Tamer, C. Sehring, M. Meißner, S. Schlie-Wolter, B.N. Chichkov, Water-soluble photopolymerizable chitosan hydrogels for biofabrication via two-photon polymerization, Acta Biomater. 18 (2015) 186–195. https://doi.org/10.1016/j.actbio.2015.02.025.

[29] Y. Shen, H. Tang, X. Huang, R. Hang, X. Zhang, Y. Wang, X. Yao, DLP printing photocurable chitosan to build bio-constructs for tissue engineering, Carbohydr. Polym. 235 (2020) 115970. https://doi.org/10.1016/j.carbpol.2020.115970.
[30] G. Melilli, I. Carmagnola, C. Tonda-Turo, F. Pirri, G. Ciardelli, M. Sangermano, M. Hakkarainen, A. Chiappone, DLP 3D Printing Meets Lignocellulosic Biopolymers: Carboxymethyl Cellulose Inks for 3D Biocompatible Hydrogels, Polymers 12 (2020) 1655. https://doi.org/10.3390/polym12081655.
[31] D. Cafiso, A.A. Septevani, C. Noè, T. Schiller, C.F. Pirri, I. Roppolo, A. Chiappone, 3D printing of fully cellulose-based hydrogels by digital light processing, Sustain. Mater. Technol. 32 (2022) e00444. https://doi.org/10.1016/j.susmat.2022.e00444.
[32] H. Yao, J. Wang, S. Mi, Photo Processing for Biomedical Hydrogels Design and Functionality: A Review, Polymers 10 (2017) 11. https://doi.org/10.3390/polym10010011.
[33] M.S. Rahman, M.S. Hasan, A.S. Nitai, S. Nam, A.K. Karmakar, M.S. Ahsan, M.J.A. Shiddiky, M.B. Ahmed, Recent Developments of Carboxymethyl Cellulose, Polymers 13 (2021) 1345. https://doi.org/10.3390/polym13081345.
[34] S. Dutta, P. Samanta, D. Dhara, Temperature, pH and redox responsive cellulose based hydrogels for protein delivery, Int. J. Biol. Macromol. 87 (2016) 92–100. https://doi.org/10.1016/j.ijbiomac.2016.02.042.
[35] H.A. Lin, M.S. Gupta, D.M. Varma, M.L. Gilchrist, S.B. Nicoll, Lower crosslinking density enhances functional nucleus pulposus-like matrix elaboration by human mesenchymal stem cells in carboxymethylcellulose hydrogels: Crosslinking Density Impacts hMSC Chondrogenesis, J. Biomed. Mater. Res. A 104 (2016) 165–177. https://doi.org/10.1002/jbm.a.35552.
[36] L. Soullard, P.-A. Bayle, C. Lancelon-Pin, S. Rolere, I. Texier, B. Jean, G. Nonglaton, Optimization of the methacrylation of carboxymethylcellulose and use for the design of hydrogels and cryogels with controlled structure and properties, Cellulose (2023). https://doi.org/10.1007/s10570-023-05266-w.
[37] N. Abbasi, S. Hamlet, R.M. Love, N.-T. Nguyen, Porous scaffolds for bone regeneration, J. Sci. Adv. Mater. Devices 5 (2020) 1–9. https://doi.org/10.1016/j.jsamd.2020.01.007.
[38] W. Tomal, J. Ortyl, Water-Soluble Photoinitiators in Biomedical Applications, Polymers 12 (2020) 1073. https://doi.org/10.3390/polym12051073.
[39] T. Zandrini, N. Liaros, L.J. Jiang, Y.F. Lu, J.T. Fourkas, R. Osellame, T. Baldacchini, Effect of the resin viscosity on the writing properties of two-photon polymerization, Opt. Mater. Express 9 (2019) 2601. https://doi.org/10.1364/OME.9.002601.
[40] L. Soullard, F. Pradalié, B. Labat, C. Lancelon-Pin, G. Nonglaton, S. Rolere, I. Texier, B. Jean, Methacrylated Cellulose Nanocrystals as Fillers for the Development of Photo-Cross-Linkable Cytocompatible Biosourced Formulations Targeting 3D Printing, Biomacromolecules 24 (2023) 6009–6024. https://doi.org/10.1021/acs.biomac.3c01090.
[41] D. Miedzińska, R. Gieleta, A. Popławski, Experimental Study on Influence of Curing Time on Strength Behavior of SLA-Printed Samples Loaded with Different Strain Rates, Materials 13 (2020) 5825. https://doi.org/10.3390/ma13245825.
[42] O. Chaudhuri, J. Cooper-White, P.A. Janmey, D.J. Mooney, V.B. Shenoy, Effects of extracellular matrix viscoelasticity on cellular behaviour, Nature 584 (2020) 535–546. https://doi.org/10.1038/s41586-020-2612-2.
[43] J. da Silva, R. Fracacio, Toxicological and ecotoxicological aspects of tartrazine yellow food dye: a literature review, Rev. Bras. Ciênc. Ambient. Online 56 (2020) 137–151. https://doi.org/10.5327/Z21769478746.
[44] P. Amchova, H. Kotolova, J. Ruda-Kucerova, Health safety issues of synthetic food colorants, Regul. Toxicol. Pharmacol. 73 (2015) 914–922. https://doi.org/10.1016/j.yrtph.2015.09.026.
[45] K.A. Sindhu, R. Prasanth, V.K. Thakur, Medical Applications of Cellulose and its Derivatives: Present and Future, in: V.K. Thakur (Ed.), Nanocellulose Polym. Nanocomposites, John Wiley & Sons, Inc., Hoboken, NJ, USA, 2014: pp. 437–477. https://doi.org/10.1002/9781118872246.ch16.
[46] Y. Shi, D. Xiong, Y. Liu, N. Wang, X. Zhao, Swelling, mechanical and friction properties of PVA/PVP hydrogels after swelling in osmotic pressure solution, Mater. Sci. Eng. C 65 (2016) 172–180. https://doi.org/10.1016/j.msec.2016.04.042.

[47] G. Della Giustina, A. Gandin, L. Brigo, T. Panciera, S. Giulitti, P. Sgarbossa, D. D'Alessandro, L. Trombi, S. Danti, G. Brusatin, Polysaccharide hydrogels for multiscale 3D printing of pullulan scaffolds, Mater. Des. 165 (2019) 107566. https://doi.org/10.1016/j.matdes.2018.107566.

SUPPLEMENTARY DATA

Towards the 3D printing of innovative hydrogel scaffolds through vat polymerization techniques using methacrylated carboxymethylcellulose aqueous formulations

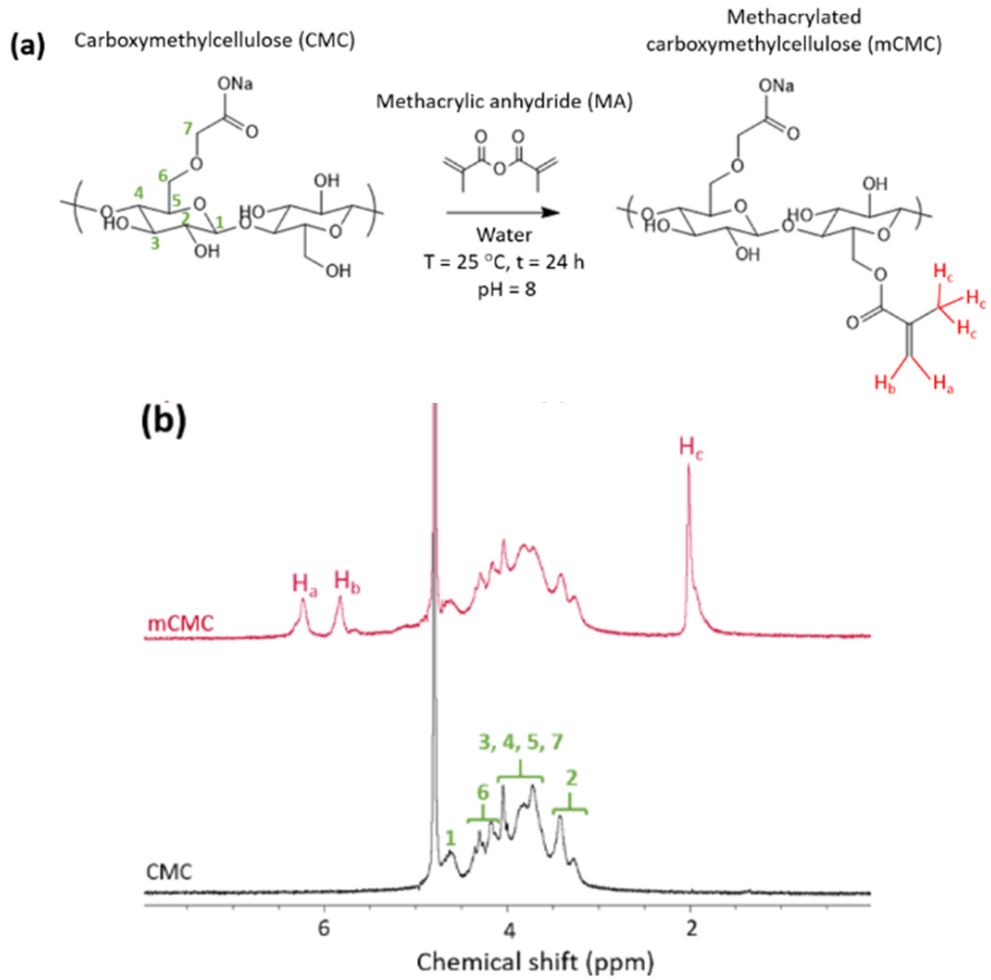

Figure S1. (a) Scheme of the methacrylation of CMC with MA in water at 25 °C to yield mCMC. (b) ^{1}H NMR spectra for initial CMC (black spectrum) and mCMC with a DM of 50% (red spectrum) obtained using a molar ratio of 2.48 between MA and CMC hydroxyl groups.

Photo-crosslinkable methacrylate groups were successfully grafted onto CMC using the reaction between methacrylic anhydride (MA) and the polymer hydroxyl groups (Fig. S1a). The samples were characterized by liquid ^{1}H NMR and compared to raw CMC (Fig. S1b) to determine the degree of methacrylation. Protons of the CMC unit are located in the bulk between 2.8 and 4.7 ppm, and account for 8.4 protons considering a DS of 0.7. For mCMC samples, three additional peaks corresponding to the vinyl (Ha: 6.0-6.4 ppm, Hb: 5.65-6.0 ppm) and methyl (Hc: 1.7 - 2.2 ppm) protons of the methacrylate groups were also found after purification, indicating that methacrylation occurred under our experimental conditions. Please see : http://dx.doi.org/10.3390/polym2030252, for more details.

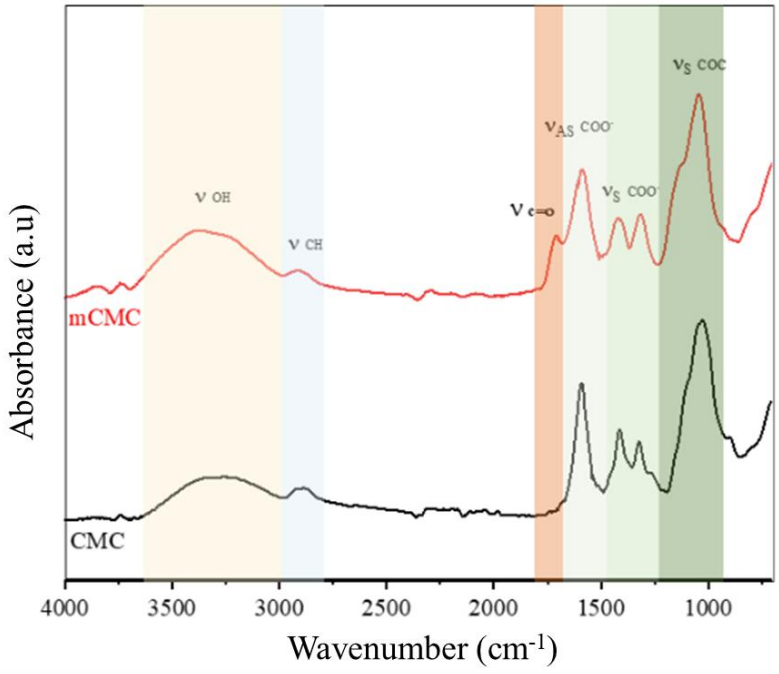

Figure S2. FT-IR spectra of carboxymethylcellulose (CMC, black spectrum) and methacrylated carboxymethylcellulose (mCMC) with a DM of 50% (red spectrum) obtained using a molar ratio of 2.48 between MA and CMC hydroxyl groups.

Attenuated total reflection (ATR) Fourier transform infrared (FT-IR) spectroscopy measurements were carried out using a MIRacle 10 instrument (Shimadzu, Japan) to analyze the characteristic chemical bonds and functions of the CMC and mCMC samples. Absorption spectra were acquired over the 4000-550 cm^{-1} wavenumber range (64 scans, 4 cm^{-1} resolution).

CMC has a broad band between 3000 and 3650 cm^{-1} corresponding to OH groups. The υ vibration band of the C-H bonds appears at 2907 cm^{-1}. The antisymmetrical (1590 cm^{-1}) and symmetrical (1407 cm^{-1} and 1312 cm^{-1}) υ vibration bands correspond to those of carboxylate groups (COO^-). At 1043 cm^{-1} appears the band characteristic of the C-O-C bonds of the glucosic units of CMC and mCMC.

Finally, the appearance of a band corresponding to the carbonyl group (C=O) of the methacrylate at 1705 cm^{-1} on the mCMC spectra, compared with the CMC spectrum, qualitatively demonstrates the success of methacrylation.

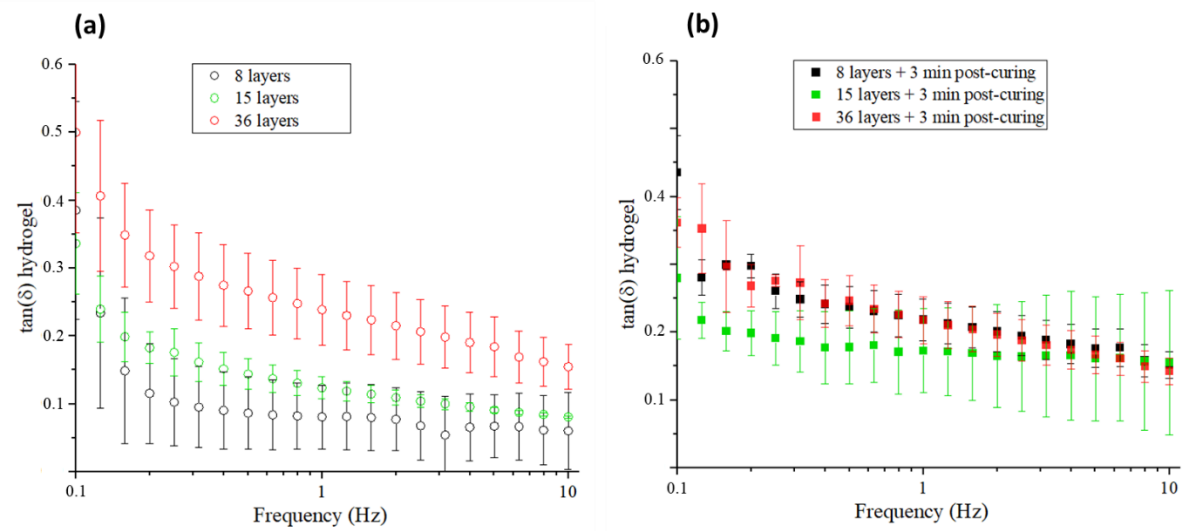

Figure S3. Evolution of the loss factor tan(δ) measured between 0.1 and 10 Hz and at 1 % strain at 25 °C, for 4 mm-thick hydrogels printed by DLP from the LAP-2 formulation with exposure times of 5 s for the first layer and 4 s for subsequent layers, and thicknesses of 500 µm for the first layer and 100 µm (36 layers, A1), 250 µm (15 layers, A2) and 500 µm (8 layers, A3) for subsequent layers, respectively, **(a)** before and **(b)** after a 3 min UV post-curing (365 nm + 405 nm, 6 $mW.cm^{-2}$).

Table S1. Influence of different printing parameters on the structure of pyramidal hydrogels (model B) printed by DLP from the LAP-2 formulation containing a concentration of 2 wt% mCMC with a DM of 34 % and 0.15 wt% LAP. The dimensions of the structure are constant (14 x 14 x 8 mm^3 ; L x l x h) and correspond to a step height and width of 2 mm.

Range	Exposure time for the 1st layer (s)	Exposure time for subsequent layers (s)	Crosslinked layer thickness (µm)*	Final state of printed hydrogel
1	5	3	100	Collapsing
2	5	3	500	Collapsing
3	5	4	100	Peripheral crosslinking
4	5	4	250	Peripheral crosslinking
5	5	4	500	Figure 2e
(2)	5	3	500	Collapsing
(5)	5	4	500	Figure 2e
6	5	5	500	Low peripheral crosslinking
7	5	10	500	Peripheral crosslinking
(5)	5	4	500	Figure 2e
8	10	4	500	Peripheral crosslinking at the base

* The crosslinked layer thickness corresponds to the Z movement of the platform, between each layer insolation.

It was observed that an exposure time of 10 seconds caused peripheral polymerization, resulting in the formation of cured zones outside the exposed area. This peripheral polymerization occured gradually throughout the thickness of the same step and became less visible from the first to the last layer. The reason lied in UV rays penetrating layers that were already crosslinked when a new layer was formed. Indeed, layer thicknesses of 100 to 500 µm were printed in the case of these pyramids (Table S1). However, it was observed that an exposure of only 4 seconds without limiting the thickness to be exposed could cure layers up to 3.5 mm thick (Figure S2). Thus, during the exposure of a new layer with a maximum thickness of 500 µm, the previous layers were also exposed. For example, when printing the same level of the pyramid with a layer thickness of 500 µm, the first layer (5 s) was also exposed during the printing of the following 3 layers. Also, for an exposure time of 10 seconds per layer, the total exposure times for layers 1 to 4 were 35 s, 30 s, 20 s and 10 s, respectively. Peripheral polymerization was therefore more significant on layer 1 and decreased with subsequent layers.

With layer thicknesses of 500 µm and exposure times of 4 seconds, peripheral polymerization was almost negligible over the thickness of the same level. However, the phenomenon was slightly observable at the interface between two layers of different surfaces. Furthermore, the phenomenon of peripheral polymerization intensified when the layer thickness was lower because the exposure time was multiplied by the number of layers. To mitigate this phenomenon, it is possible to reduce the exposure time for thinner layer thicknesses. However, with a 3-second exposure time, the cured layer thickness was not sufficiently resistant to support the layer that collapsed during the back-and-forth movement of the platform, before the formation of the next layer.

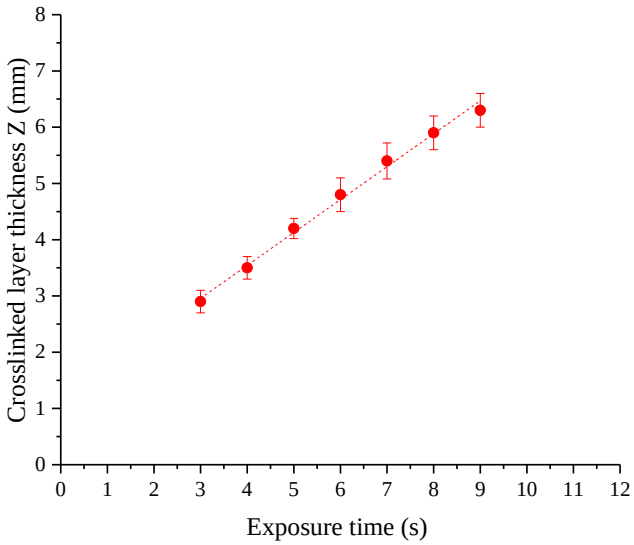

Figure S4. Evolution of the crosslinked layer thickness as a function of the UV exposure time, for the LAP-2 formulation containing 2 wt% mCMC with a DM of 34 % and 0.15 wt% LAP.

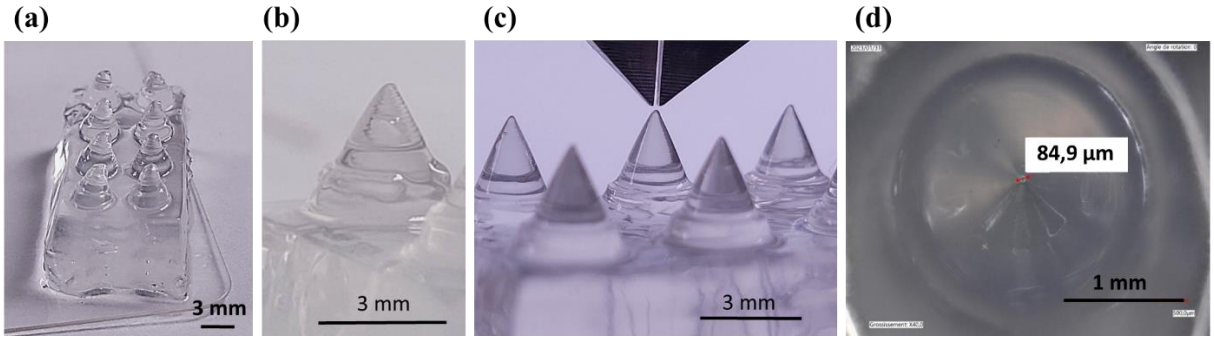

Figure S5. Conical hydrogels on a flat base (Model C) printed by DLP from the LAP-2 formulation containing 2 wt% mCMC with a DM of 34 % and 0.15 wt% LAP, with an exposure time of 4 s per layer and with a layer thickness (Z) of 500 µm **(a)**, 200 µm **(b)**, 100 µm **(c)** and 50 µm **(d)**.

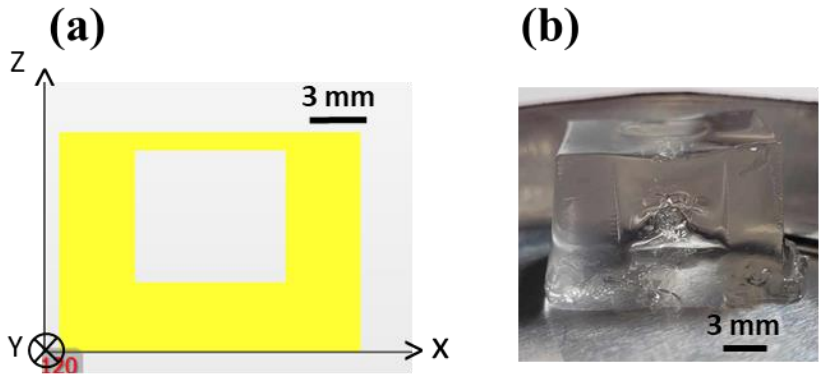

Figure S6. (a) CAD model of a hollow parallelepiped with external dimensions of 10.13 x 15.10 x 15.00 mm^3 (L x W x H). **(b)** Corresponding hydrogel printed by DLP from the LAP-2 formulation containing 2 wt% mCMC with a DM of 34 % and 0.15 wt% LAP, with a layer thickness of 500 µm and an exposure time of 5 s for the first layer and 4 s for subsequent layers.

Several limitations appeared when printing a hollow parallelepiped hydrogel by DLP, trying to optimize resolution in the Z direction:

(1) If the upper part of the parallelepiped is too thick, peripheral polymerization along the Z-axis led to the blocking of the cavity.

(2) If the upper part of the parallelepiped was too thin (Figure S4a), there were not enough printed layers for the upper wall to hold. Therefore, taller walls were needed, and a compromise on the thickness of the upper wall has to be found to avoid peripheral curing while maintaining sufficient mechanical properties.

(3) Furthermore, if the walls along the Z-axis were too tall, the hydrogel collapsed. Thus, a sufficient width for these walls had to be determined to maintain the shape of the printed hydrogel.

(4) However, the dimensions of the cavity in X and Y had been sufficient to prevent peripheral polymerization from closing the cavity (Figure S4b).

In summary, designing the piece to print a hydrogel that was self-standing and presented a cavity perpendicular to the Z-axis was challenging. Printing a scaffold by DLP was therefore not possible using the LAP-2 formulation.

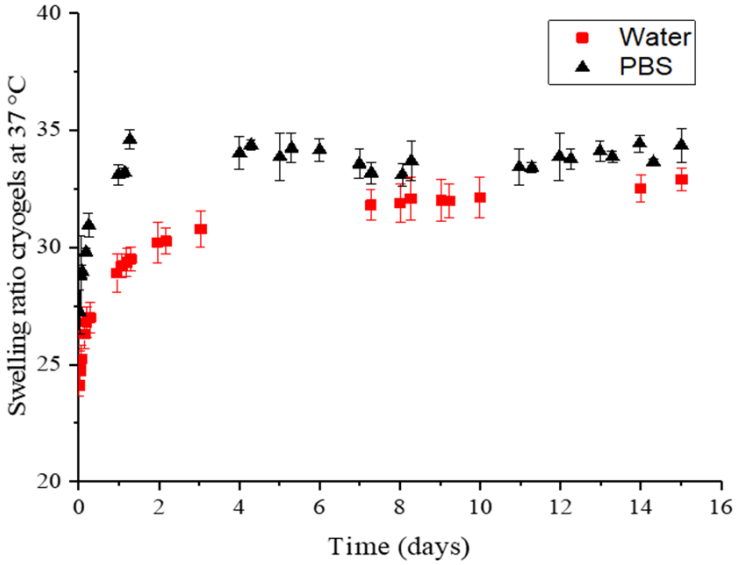

Figure S7. Evolution of the swelling ratio of A2 cryogels with time immerged in water or PBS at 37 °C. A2 hydrogels were printed with 250 µm layers exposed for 4 s (500 µm and 5 s for the first layer) from the LAP-2 formulation containing a concentration of 2 wt% mCMC with a DM of 34 % and 0.15 wt% LAP, then post-cured for 3 min.

Table S2. Composition of mCMC formulations containing I2959 or LAP as photoinitiator, used in preliminary TPP printing trials.

mCMC		Photo-initiator		Printing parameters		
DM (%)	**Concentration (wt%)**	**Name**	**Concentration (wt%)**	**Power (mW)**	**Speed (µm/s)**	**Polymerization**
34	2	LAP	0.15	11	187.5	No
	3		0.22	7.2	93.5	
	4		0.31	6.7	37.5	
				6.7	18.7	
34	2	I2959	0.12	9.7	187.5	No
				9.7	84	
	3		0.18	9.1	187.5	Low
				8.6	94	
				8.6	37	
	4		0.25	4	187.5	Insufficient for a stable hydrogel
				4.5	187.5	
				5	187.5	
50	4	I2959	0.41	4	187.5	Yes

Initial tests were carried out using formulations containing 2, 3 or 4 wt% mCMC with a DM of 34 %, as well as LAP as photoinitiator at 0.15, 0.22 and 0.31 wt%. However, no polymerization was observed under the printing conditions used.

To promote polymerization, it was necessary to increase the light power or decrease the polymerization speed. However, by increasing the time and power received by the resin, a degradation of the latter was observed, accompanied by the formation of bubbles corresponding to local boiling. This phenomenon, which exists for all photo-crosslinkable formulations, is referred to as the resin's "damage threshold". However, in the case of the mCMC formulations studied, no polymerization was observed before this threshold is reached.

Two parameters may explain the early onset of the damage threshold. Firstly, the low concentration of methacrylate groups in water-rich formulations may initially make crosslinking difficult in the voxel volume. The choice of LAP as a photoinitiator can also be blamed. At the focal point, the energy received by the formulation in the voxel corresponds to a wavelength of 266 nm. At this wavelength, LAP is at the absorbance limit, and would therefore require greater laser gain to initiate methacrylate polymerization. On the other hand, I2959 absorbs more than LAP at this wavelength, and could enable polymerization to be initiated with a laser gain lower than the damage threshold of the formulations.

For the formulation containing 3 wt% mCMC, a slight polymerization was observed, depending on the parameters used. However, this was insufficient to print complex objects. Finally, for the formulation containing 4 wt% mCMC, it was possible to obtain suitable polymerization between the polymerization threshold and the damage threshold, depending on the exposure time. However, polymerization was not sufficient to achieve adequate mechanical strength of the printed hydrogel. To improve the mechanical properties of TPP-printed hydrogels, the concentration of methacrylate groups needed to be increased. A formulation containing 4 wt% mCMC with a DM of 50 % was therefore used in the following tests.

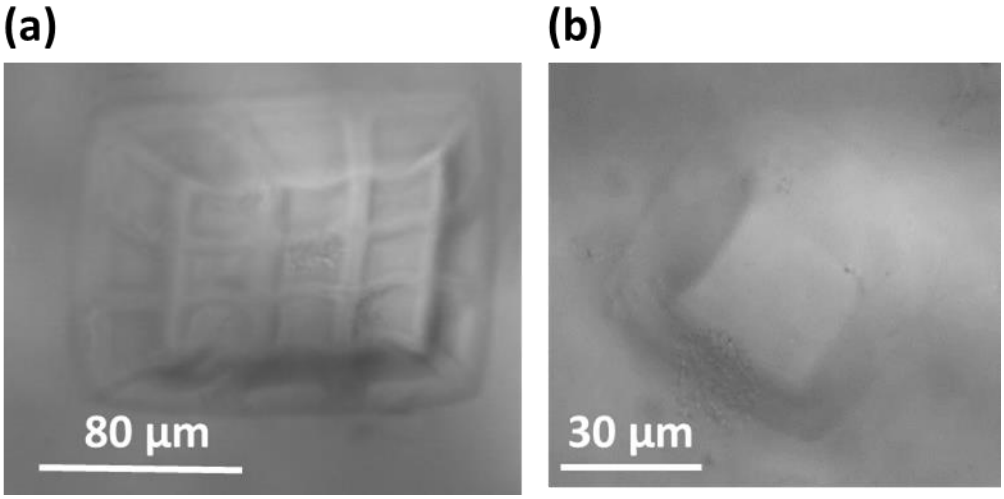

Figure S8. Images of scaffold- **(a)** and well- **(b)** shaped hydrogels printed by TPP from the IRG-4 formulation containing 4 wt% mCMC with a DM of 50 % and 0.4 wt% I2959 as photoinitiator, obtained after dehydration using Dino-lite (ref RS AM4815ZTL) at magnification x232.9. The printing was done using a 4 mW laser beam at a printing speed of 187.5 $\mu m.s^{-1}$.